*Clays and Clay Minerals*, Vol. 26, No. 1, pp. 25–40, 1978.

# OBSERVATION OF THE HYDRATED FORM OF TUBULAR HALLOYSITE BY AN ELECTRON MICROSCOPE EQUIPPED WITH AN ENVIRONMENTAL CELL

NORIHIKO KOHYAMA

National Institute of Industrial Health, Ministry of Labor
Nagao, Tama-ku, Kawasaki 213, Japan

KURIO FUKUSHIMA AND AKIRA FUKAMI

Department of Physics, College of Humanities and Sciences
Nihon University, Sakurajosui, Setagaya-ku, Tokyo 156, Japan
(*Received 29 August 1977*)

**Abstract**—The hydrated form of tubular halloysite [halloysite (10 Å)] was observed by a conventional electron microscope equipped with an environmental cell (E.C.), by which the "natural" form was revealed without dehydration of the interlayer water. This study mainly reports the selected area electron diffraction (SAED) analysis of the halloysite (10 Å) and its morphological changes by dehydration. The SAED pattern showed halloysite (10 Å) has two-layer periodicity in a monoclinic structure with the unit cell parameters of $a = 5.14$ Å, $b = 8.90$ Å, $c = 20.7$ Å, $\beta = 99.7°$, in space group $Cc$, and almost the same structure as the dehydrated form of halloysite [halloysite (7 Å)]. This means that the dehydration of the interlayer water did not greatly change or affect the structure of halloysite (10 Å). Accompanying the dehydration of the interlayer water, there appeared along the halloysite tube axis clear stripes that were about 50–100 Å in width. The diameters of the tubular particles also increased about 10%. From the results of various experiments, such as a focussing series, observation of the surface structure by the replica method, observation of end-views of the tubular particles, and others, these two phenomena were explained as follows: Halloysite crystals have "domains" along the $c$-axis direction, the thicknesses of the "domains" vary ca. 50–100 Å. They are tightly connected with each other when the halloysite is hydrated, but are separated from each other by the dehydration of the interlayer water, whereupon the stripes come into existence along the tube axis. Taking these considerations into account, a model of dehydration is proposed. Moreover, a new method of calculating the $\beta$-angle is proposed in the Appendix.

**Key Words**—Dehydration, Diffraction, Halloysite, Kaolinite, Tubular.

## INTRODUCTION

The interlayer or adsorbed water in some clay minerals, such as halloysite (10 Å),* montmorillonite, vermiculite, imogolite, allophane, etc., is quite susceptible to dehydration in dried air, in vacuum, or at moderately high temperature in the atmosphere. The dehydration or deformation of these specimens, therefore, necessarily occurs when we have observed them by conventional electron microscopy. On the other hand we can observe the wet or hydrated specimen without dehydration by optical microscopy, but the resolving power is limited and it is impossible to observe the desired details of these clay minerals. The interlayer or adsorbed water is an essential component of these clay minerals. In this sense, we have only observed a "temporary feature" instead of the "real feature" of wet and/or hydrated specimens when they are viewed by conventional electron microscopy.

Recently environmental cells have been developed that enhance the possibilities of electron diffraction analysis of minute hydrated crystals and biological paracrystals (Fukami, et al., 1974; Parsons, 1974; Dorset and Parsons, 1975). It has been confirmed also by some investigators that an environmental cell attached to a conventional transmission electron microscope is effective for observing an electron microscopic imaging of wet specimens without dehydration.

Halloysite is well known as a kaolin mineral composed of 1:1 layers, which occurs in different morphological forms, i.e., tubular and spheroidal forms. The main geological occurrence of halloysite is in soils and weathered rocks, and the relation of occurrence and morphology has been studied by a number of authors (Sudo and Ossaka, 1952; Nagasawa et al., 1969; Bates, 1971; Askenasy et al., 1973). The structure and morphology for halloysite (7 Å) has been investigated with conventional electron microscopy (Bates et al., 1954; Honjo et al., 1954; Honjo and Mihama, 1954; Souza Santos et al., 1965; Chukhrov and Zvyagin, 1966; Dixon and Mckee, 1974). The basic structure of halloysite (7 Å) was established, but that of halloysite (10 Å) has not been examined directly to date, because of the susceptibility of its interlayer water to dehydration. We successfully observed the hydrated form of tubular halloysite in an transmission electron microscope equipped with an environmental cell. This paper mainly describes the selected area electron diffraction (SAED)

*Various terms are currently used for the hydrated and the less hydrous forms of halloysite. We use the terms halloysite (10 Å) and halloysite (7 Å) to express the hydrated and the dehydrated forms of halloysite, respectively, on the basis of the recommendation of the nomenclature committee of A.I.P.E.A. at Mexico City (1975). The term halloysite, however, is occasionally used as a group name, i.e., both forms of halloysite, in this paper.

Table. 1. Evaluation of interlayer water for halloysite (10 Å).

| | Obs. (%)* | Calc. (%) |
|---|---|---|
| Halloysite (10Å) from Kusatsu | 12.3 | |
| $Al_2Si_2O_5(OH)_4 \cdot 2H_2O$ | | 12.2 |
| $Al_2Si_2O_5(OH)_4 \cdot 4H_2O$ | | 31.8 |

* : Observed value by TG, between 20°C and 300°C.

analysis of halloysite (10 Å), and the changes in morphology resulting from dehydration of its interlayer water.

## SPECIMEN

### *X-ray powder diffraction and thermal properties*

The observed specimen was a halloysite (10 Å) from Kusatsu, Gumma Prefecture, Japan, which showed tubular particles in electron micrographs. Under natural room temperature and humidity, the halloysite (10 Å) showed a strong basal reflection of 10.1 Å by X-ray powder diffraction analysis. The spacing of the basal reflection ranges from 7 to 10 Å depending upon the state of hydration. These two typical X-ray powder diffraction patterns are shown in Figure 1. The 4.44 Å peaks are strong in comparison with the first order basal reflection. These patterns are fairly characteristic of halloysite using the criterion of Brindley (1961) which requires the 4.44 Å peak to be more than half the intensity of the first order basal reflection. The strong basal reflection of 10.1 Å was largely lost when the interlayer water was dehydrated and the 7.4 Å reflection appeared clearly [halloysite (7 Å)]. This phenomenon also occured at a temperature slightly higher than the usual room temperature, and in a vacuum of about 1 Torr at room temperature for a short period. Once the interlayer water of halloysite (10 Å) was lost, it was not restored by treatment with water or ethylene glycol, that is, the dehydration is an irreversible reaction.

DTA curves showed clear endothermic peaks at about 110 and 560°C, and a sharp exothermic peak at about 990°C. TG analysis indicated about 12.3% weight loss between 20 and 300°C. This value indicates that the interlayer water of the halloysite (10 Å) exists as two water molecules per a basic formula of $Al_2Si_2O_5(OH)_4$ as shown in Table 1.

The calculated intensities of basal reflection for halloysite (10 Å) (having two water molecules per a basic formula in the interlayer) and halloysite (7 Å) (no water molecule in the interlayer) are listed in Table 2. According to Table 2, it is obvious that the first and the third order reflections of halloysite (10 Å) are comparatively strong, whereas the halloysite (7 Å) shows strong first and second order reflections.

### *Effect of temperature and humidity*

A specimen coated on a slide glass was treated for 30 minutes in a box in which the relative humidity and temperature were controlled. The temperature was held at steps ranging from 25 to 75°C. After the treatment, the specimen was X-rayed to determine the change in the basal spacing from 10 to 7 Å (Figure 2). When the relative humidity was held at 40%, halloysite (10 Å) was changed to halloysite (7 Å) at about 40°C. Under a relative humidity of 100% or slightly less, the change occurred at about 65°C. When the specimen was maintained in an oversaturated state, as in a hot water bath, the halloysite (10 Å) did not dehydrate up to about 95°C. It is revealed, therefore, that the dehydration temperature of the interlayer water in halloysite is strongly affected by the relative humidity.

## EXPERIMENTAL PROCEDURES

### *Environmental cell*

The environmental cell (E.C.) used in this study has been developed by Dr. A. Fukami, one of the authors, at his laboratory of Nihon University (Fukami and Katoh, 1972). This E.C. is a type composed of a copper-microgrid having a single hole, as is used for the conventional electron microscope, sealed by a thin film. The principle and details of various types of E.C. are described in previous papers (Fukami, et al., 1974; Fukami and Murakami, 1974; Parsons, 1974).

https://doi.org/10.1346/CCMN.1978.0260103 Published online by Cambridge University Press

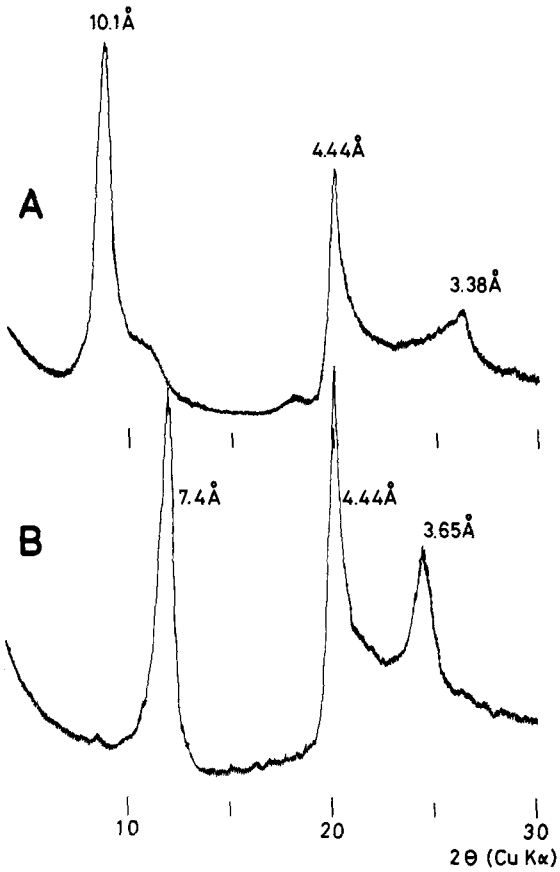


Fig. 1. X-ray powder diffraction curves for tubular halloysite of the present specimen. (A) halloysite (10 Å); (B) halloysite (7 Å).

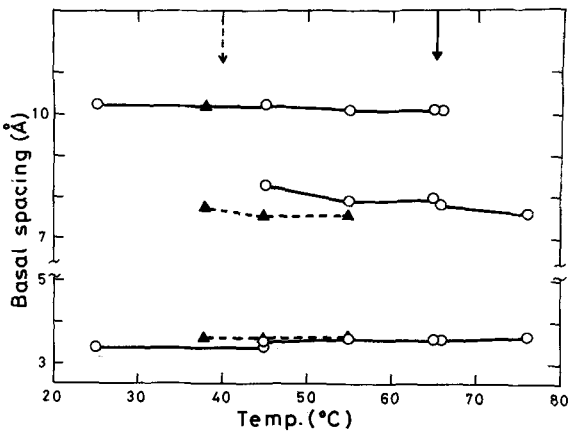


Fig. 2. Variation of basal-spacing versus the temperature and relative humidity for halloysite (10 Å). ○: relative humidity of 100% or a little under; ▲: relative humidity of 40%; →: dehydration temperature of halloysite (10 Å) in the condition of 100% or a little under of R.H.: ----→: dehydration temperature of halloysite (7 Å) in the condition of 40% R.H.

This E.C. can be set arbitrarily to gas pressures from 760 Torr to vacuum. The wet specimen was introduced into the E.C. attached to an electron microscope (JEM 7A) with an accelerating voltage of 100 kV and controlled gas pressure and relative humidity.

Specimens viewed in the conventional electron microscopes are usually damaged by the irradiating electron beam. In addition to this damage, they also are damaged by the dissociation products, such as ions or radicals generated by the electron beam striking against gas or water molecules in the E. C. Quantitative investigations of these damages have been performed (Fukami et al., 1974) where it was found that the electron dosage (ampere × time/cm$^2$) which did not damage biological specimens was about $10^{-3}$ coulomb/cm$^2$. Moreover, the specimen temperature when exposed to the electron beam in the E.C. was examined semiquantitatively using the dehydration phenomenon of halloysite (10 Å) in this study.

*Observation by environmental cell*

A drop of the hydrated halloysite suspension was placed on a single-hole copper-microgrid sealed by a thin carbon film. One minute was allowed for crystals to precipitate from suspension onto the microgrid surface before the E.C. was inserted into the electron microscope.

Electron microscopic observation was performed by a conventional electron microscope (JEM 7A) equipped with the E.C. and operated at 100 kV. Generally, in this study, halloysite (10 Å) particles were observed under a water-saturated atmosphere at less than 100 Torr (abbreviated as E.C. (air)). Next, the atmosphere was exhausted to vacuum (abbreviated as E.C.(vac)). The same particles were observed also in vacuum. This process is called "dynamic observation."

Electron microscope images of "dynamic observation" were taken using an industrial X-ray film (Fuji Ix-150). The other ordinary images, such as Figures 13 and 14, were taken by a usual film for electron microscopy.

## RESULTS AND DISCUSSION

*Estimation of the specimen temperature*

We estimated the specimen temperature in the electron microscope with the E.C. from the dehydration temperature of interlayer water of halloysite (10 Å). SAED patterns of halloysite (10 Å) in the state of E.C. (air) were changed to that of halloysite (7 Å) by raising only the electron dosage. This experiment was performed with as large a number of halloysite particles as possible in the selected area.

SAED patterns of halloysite (10 Å) were obtained with current densities at the specimen of about $10^{-4}$–$10^{-3}$amp/cm$^2$ for periods of 2 minutes exposure under the condition of E.C.(air). But the specimens were present under the condition of E.C.(air) for about 10 minutes in all, which was needed for researching, de-

https://doi.org/10.1346/CCMN.1978.0260103 Published online by Cambridge University Press

Table 2. Calculated intensity of halloysite (10 Å) and halloysite (7 Å).

| | Halloysite (10Å) | | Halloysite (7Å) | |
|---|---|---|---|---|
| | $Al_2Si_2O_5(OH)_4 \cdot 2H_2O$ | | $Al_2Si_2O_5(OH)_4$ | |
| | d(Å) | $I/I_0$ | d(Å) | $I/I_0$ |
| 002 | 10.20 | 100 | 7.20 | 100 |
| 004 | 5.10 | 3 | 3.60 | 116 |
| 006 | 3.40 | 10 | 2.40 | 30 |
| 008 | 2.55 | 3 | 1.80 | 10 |
| 00·10 | 2.04 | 5 | 1.44 | 12 |

ciding and focussing the visual field, and for exposure of the images. Under the same condition of E.C.(air), the current densities at the specimen were increased in several steps, and the basal diffractions were observed as streaks from 10 to 8 Å with about $10^{-2}$amp/cm$^2$ for periods of 2 minutes exposure. With about $10^{-1}$–$10^{-2}$amp × 2 min/cm$^2$ the basal diffraction spots and ring of 7.4 Å were obtained. It is obvious that the basal spacing of the halloysite correlates with the electron dosage at the specimen. The shrinkage of the basal spacing that is derived from dehydration of the interlayer water will be changed as a result of raising the temperature in the E.C. by exposure to the electron beam. From these results, the relation between the specimen temperature and the electron dosage at the specimen in the E.C. was estimated. Under the condition of E.C.(air), the transition temperature at which the halloysite changed from the 10 Å phase to the 7 Å phase was estimated as about 65°C because it occurred at about 65°C in the case of 100% relative humidity, and at about 40°C in the case of 40% relative humidity.

*SAED analysis of halloysite (10 Å) and halloysite (7 Å)*

SAED patterns of a single crystal of halloysite (10 Å) could be obtained under the water-saturated air condition, E.C. (air), with current density at the specimen of approximately $10^{-4}$amp/cm$^2$ and exposed for a period of 2 minutes (Figure 3). This pattern shows no change during exposure for a period of 10 minutes. Then, "dynamic observation" was applied and the same particle was observed in vacuum. The SAED pattern obtained under E.C. (vac) is shown in Figure 4, which is the same pattern usually observed by conventional electron microscopy. The characteristic feature of the SAED pattern from a single crystal of halloysite is that it contains reflections corresponding to two zones of *hkl* and *h0l*. This is due to the full rotational symmetry arising from the cylindrical character of the "single" crystal. The orientation of the crystal axes is obvious from the diffraction spots in Figures 3 and 4, that is, the horizontal direction is the $b^*$-axis and the $a^*$- and $c^*$-axes are perpendicular to the $b^*$-axis.

Generally, SAED patterns from cylindrical crystals, such as halloysite or chrysotile, show a tendency for *hkl* reflections to appear as streaky diffraction spots and *h0l* as sharp diffraction spots. The present specimen shows essentially this relationship. Honjo et al. (1954) and Honjo and Mihama (1954) studied many single crystals of halloysite or "tubular kaolin" by electron microscopy and reported that most of the crystals showed the fiber axis to be the $b^*$-direction, with the $a^*$- and $c^*$-directions perpendicular to $b^*$, as in the present study.

Microdensitometric traces along the basal reflections were performed for the SAED pattern of halloysite (10 Å) and halloysite (7 Å) as shown in Figure 5. The basal reflections of halloysite (10 Å) were observed clearly at 10.2 Å and coincided with that of the halloysite (10 Å) observed by X-ray powder diffraction analysis in the natural wet state (Figure 1), which indicated that the SAED analysis was performed without dehydration of the interlayer water of halloysite (10 Å). On the other hand, microdensitometric traces for the SAED pattern obtained in the condition of E.C. (vac) shows 7.4 Å and 3.7 Å basal reflections (Figure 5,B). This shows that the interlayer water of the halloysite (10 Å) is completely dehydrated.

Clear basal reflections of 9.9 Å, 8.6 Å, 7.9 Å, and 7.3 Å could be observed in a single crystal at one time as

https://doi.org/10.1346/CCMN.1978.0260103 Published online by Cambridge University Press

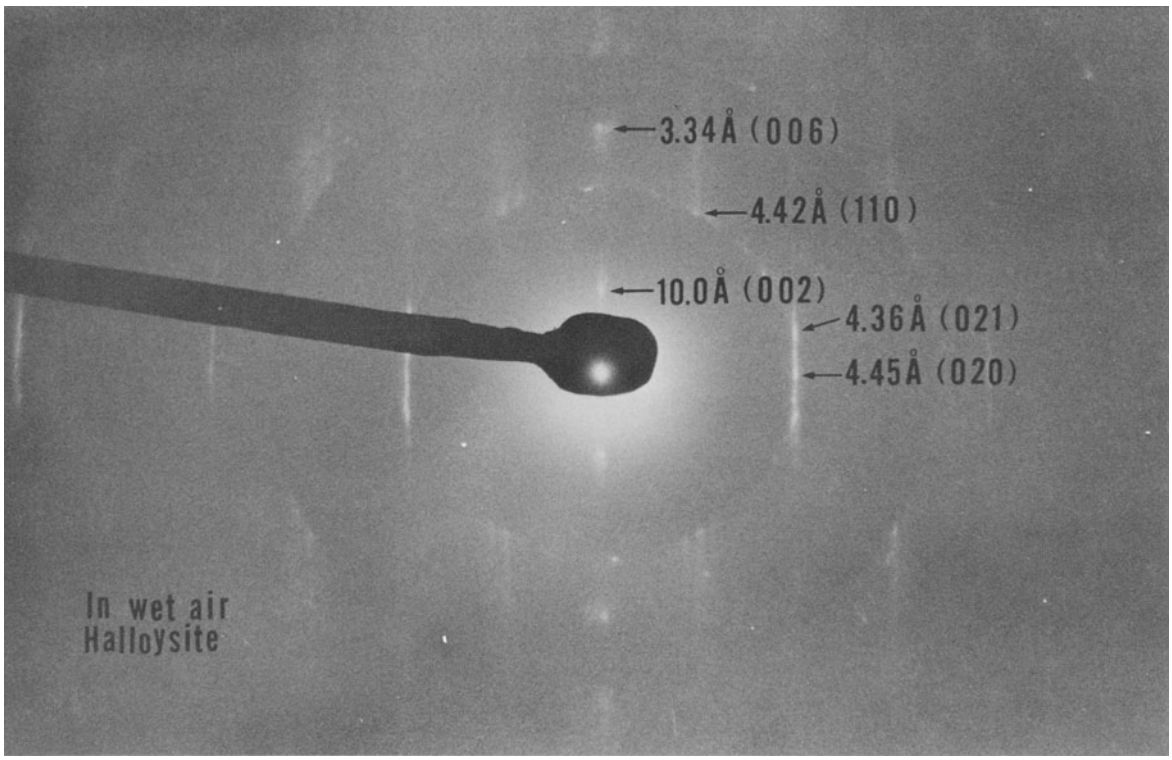


Fig. 3. SAED pattern of a single crystal of halloysite (10 Å) obtained by electron microscope with E.C. The condition in E.C.—water-saturated air condition with 80 Torr; Current densities—about $10^{-4}$ amp/cm² for 2 minutes exposure.

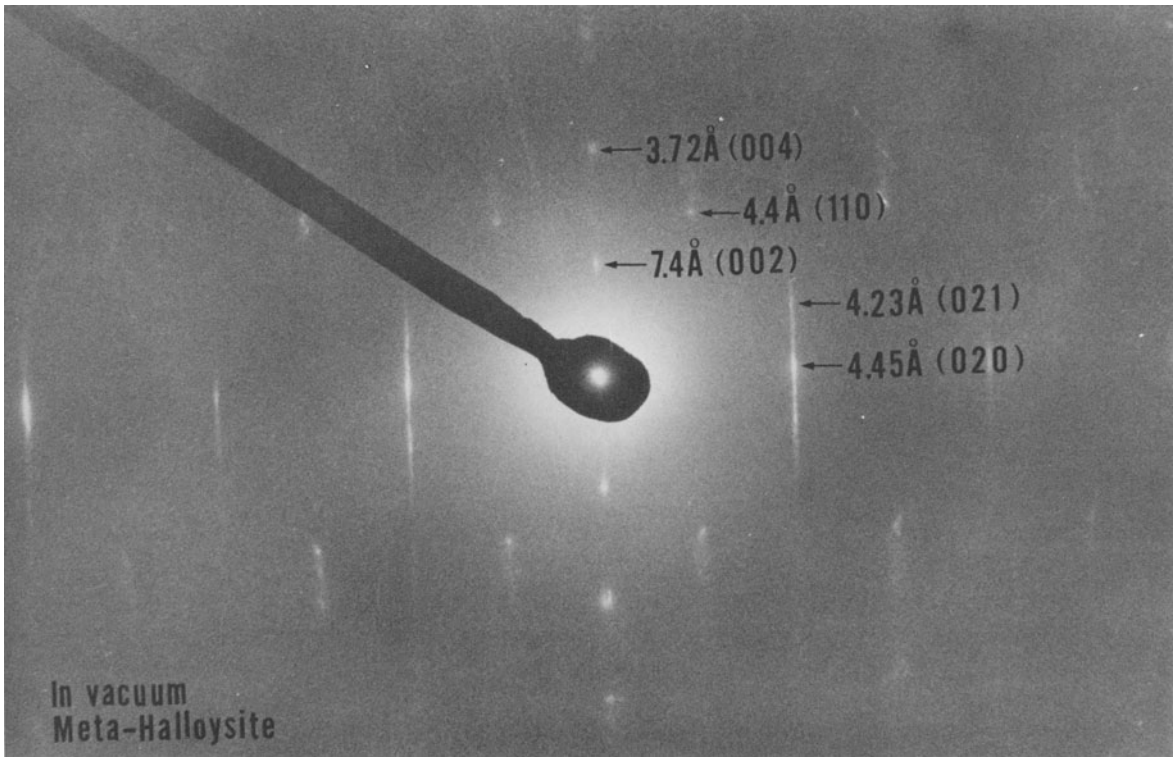


Fig. 4. SAED pattern of a single crystal of halloysite (7 Å) obtained by electron microscopy with E.C. The condition in E.C.—vacuum condition with $10^{-5}$ Torr; Current densities—about $10^{-4}$ amp/cm² with 2 minutes exposure.

https://doi.org/10.1346/CCMN.1978.0260103 Published online by Cambridge University Press

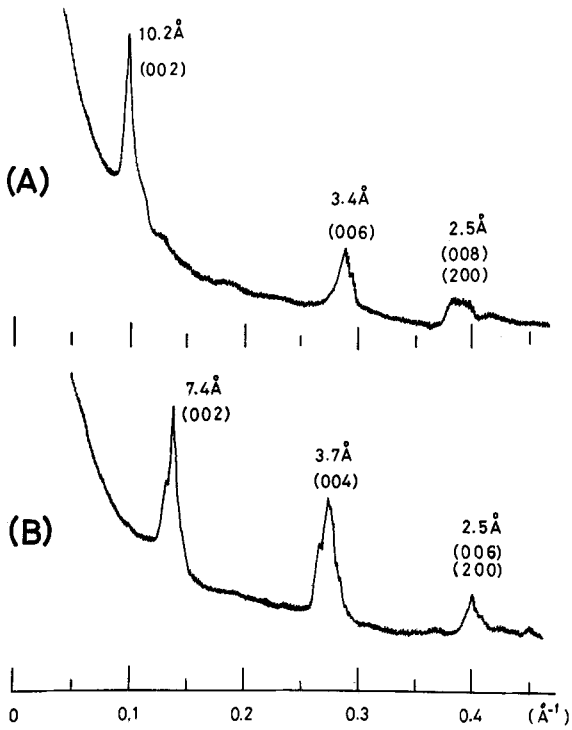


Fig. 5. Microdensitometer traces along with the [$h0l$] direction on the SAED patterns. (A) for halloysite (10 Å); (B) for halloysite (7 Å).

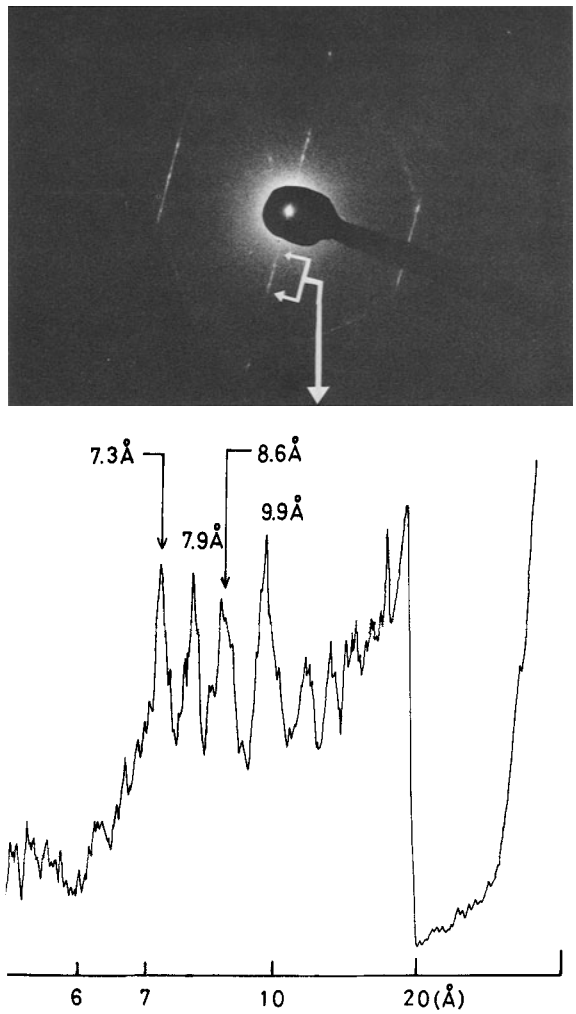


Fig. 6. SAED pattern and the microdensitometer trace of a single halloysite crystal, showing an intermediate state of the fully hydrated and the fully dehydrated form of halloysite. Microdensitometer trace along with [00$l$] direction.

shown in Figure 6, which shows an intermediate state between fully hydrated and fully dehydrated halloysite. A broad basal reflection ranging from 10 to 7 Å is often recognized in X-ray powder diffraction, but it had not been obvious previously whether the particles of hydrated and dehydrated halloysite existed as a mechanical mixture in the powder specimen or whether both hydrated and dehydrated parts coexisted in one halloysite particle. This result reveals that the partial dehydration occurs in one halloysite particle and that each phase contributes to the electron diffraction. This means that a single crystal of an halloysite particle can exist at an intermediate state between the fully hydrated and the fully dehydrated forms, and that most of the layers in the crystal make a random interstratified structure between halloysite (10 Å) and halloysite (7 Å).

The (020) diffraction in both SAED patterns of halloysite (Figures 3 and 4) appears at 4.45 Å, which indicates that $b_0$ = 8.90 Å, and the neighboring diffraction spot appears perpendicular to the $b^*$-direction at about twice the spacing of the first order basal reflection. Microdensitometric traces for SAED patterns of both the halloysite (10 Å) and the halloysite (7 Å) were performed along the (02$l$) direction as shown in Figure 7. The upper trace (A) is for halloysite (10 Å) and the lower (B) for halloysite (7 Å). The distance between the (020) diffraction spot and its nearest neighbor is about 20 Å for halloysite (10 Å) and is 14.6 Å for halloysite (7 Å). These values are just double the spacing of the first order basal diffraction spot in each case. Therefore, we index the spot adjacent to (020) as (021) and the first basal diffraction spot as (002). There appear two small peaks between 020 and 021 (Figure 7). It is ambiguous whether they are ghost peaks or the type of 02$l$. When they are of the latter, the higher ordering in the layer stacking sequence than the two-layer periodicity can be considered. But these small peaks seem to be ghost ones judging from the tolerance of microdensitometric trace and some other features. $l$-index numbers of (02$l$) thus appear as odd numbers, while (00$l$) are even $l$-numbers. From these results, we could confirm that both halloysite (10 Å) and halloysite (7 Å) have a monoclinic structure with two-layer periodicity.

Previously, two-layer periodicity had been reported by some investigators (Honjo et al., 1954; Honjo and Mihama, 1954; Souza Santos et al., 1965; Chukhrov and

https://doi.org/10.1346/CCMN.1978.0260103 Published online by Cambridge University Press

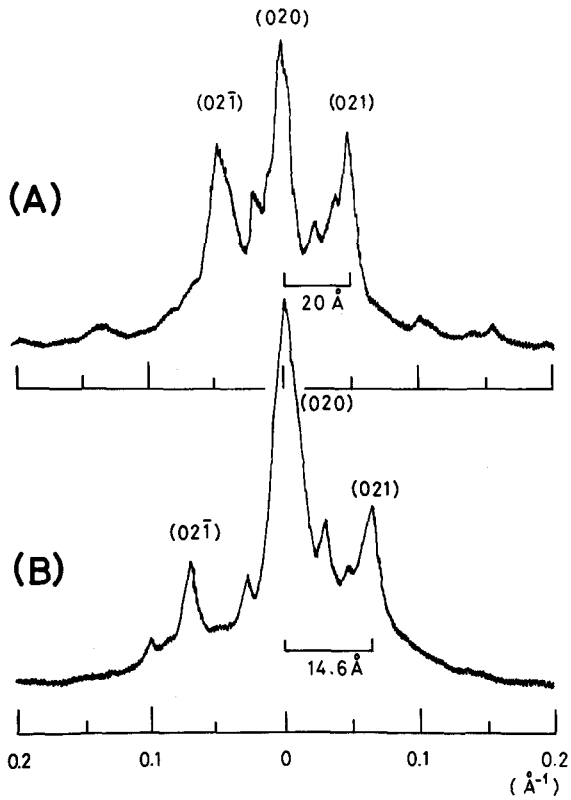


Fig. 7. Microdensitometer traces along [02$l$] direction on the SAED patterns. (A) for halloysite (10 Å); (B) for halloysite (7 Å).

Zvyagin, 1966) for halloysite (7 Å). They were, however, all for the dehydrated form because the specimens had been dehydrated in the high vacuum of the electron microscope. In this study, we have obtained SAED analysis for tubular halloysite (10 Å) and have shown a monoclinic structure with two-layer periodicity in both halloysite (10 Å) and halloysite (7 Å).

Indices for SAED patterns from halloysite (10 Å) and halloysite (7 Å) are shown in Figure 8. The arrows indicate a shift of a diffraction spot resulting from dehydration. As the diffraction patterns are otherwise similar, it is considered that the structure of both states is scarcely changed by the dehydration of the interlayer water except for the shrinkage of the basal spacing.

The SAED patterns for both halloysite (10 Å) and halloysite (7 Å) agree with the extinction conditions of space groups $Cc$ and $C2/c$. These are:

$$h\,k\,l : h + k = 2n$$
$$h\,0\,l : l = 2n; (h = 2n)$$
$$0\,k\,0 : (k = 2n).$$

They do not agree with that of the space group $C2/m$. As kaolin minerals have no center of symmetry in the unit cell, the space group of halloysite (10 Å) and halloysite (7 Å) must be $Cc$ ($C_s^4$). Parameter measurements on these specimens with a gold standard give the following values:

Halloysite (10 Å); $a = 5.14 \pm 0.04$ Å
$b = 8.90 \pm 0.04$ Å
$c = 20.7 \pm 0.1$ Å
$\beta = 99.7°$†
Halloysite (7 Å); $a = 5.14 \pm 0.04$ Å
$b = 8.90 \pm 0.04$ Å
$c = 14.9 \pm 0.1$ Å
$\beta = 101.9°$†.

They are given in Table 3 with some previous data for halloysite (7 Å) and other kaolin minerals (kaolinite, dickite, and nacrite). $\beta$-angles obtained for the present specimen, halloysite (10 Å) and halloysite (7 Å), are 99.7° and 101.9°, respectively. If it can be assumed that the stacking sequence of kaolinite layers, a component layer of halloysite, was maintained with no change through the dehydration, the $\beta$-angle of the halloysite (10 Å), i.e., 99.7°, would increase to about 104° because the basal-spacing shrinks about 30% from 20 Å to 14 Å. The observed $\beta$-angle in the present study is 101.9°, which is smaller than the predicted value of 104°, but the observation error for the $\beta$-angle is about ±1°, so that the observed increase in value for the $\beta$-angle with dehydration is reasonable.

The structure of kaolinite was first established by Brindley and Robinson (1946) and Brindley and Nakahira (1958). After that, Drits and Kashev (1960) and Zvyagin (1960) examined kaolinite closely by X-ray and electron diffraction, respectively, and reported more precise structures. On the other hand, the structure of dickite was examined in considerable detail by Newnham and Brindley (1956) and Newnham (1961) because a larger crystal could be obtained easily. The cell parameters are also shown in Table 3.

According to the latter authors, the vacant site of Al ions in the octahedral sheets of dickite alternates between C and B in successive layers to create a two-layer monoclinic structure, and the $\beta$-angle shows about 97°. In kaolinite each octahedral sheet is identical and all of the vacant sites are in C or B (A site was also reported rarely) throughout the layers, and the $\beta$-angle takes about 104°. Bailey (1963), however, proposed a modified direction of the $z$-axis for dickite which would make $\beta$ similar to that of kaolinite, i.e., $\beta = 104°$. It is, therefore, difficult to identify only by the value of $\beta$-angle whether the kaolinite layers in an halloysite crystal alternate as a sequence of a kaolinite type or as a dickite type or as the other type.

Chukhrov and Zvyagin (1966) reported that halloysite (7 Å) has the layer stacking sequence $\sigma_3\tau + \sigma_3\tau$

†These $\beta$-angles were calculated from each SAED patterns, respectively, following the new method developed by N. Kohyama, one of the authors. The calculation makes use of rotational symmetry of the tubular crystal which appears in the Appendix.

https://doi.org/10.1346/CCMN.1978.0260103 Published online by Cambridge University Press

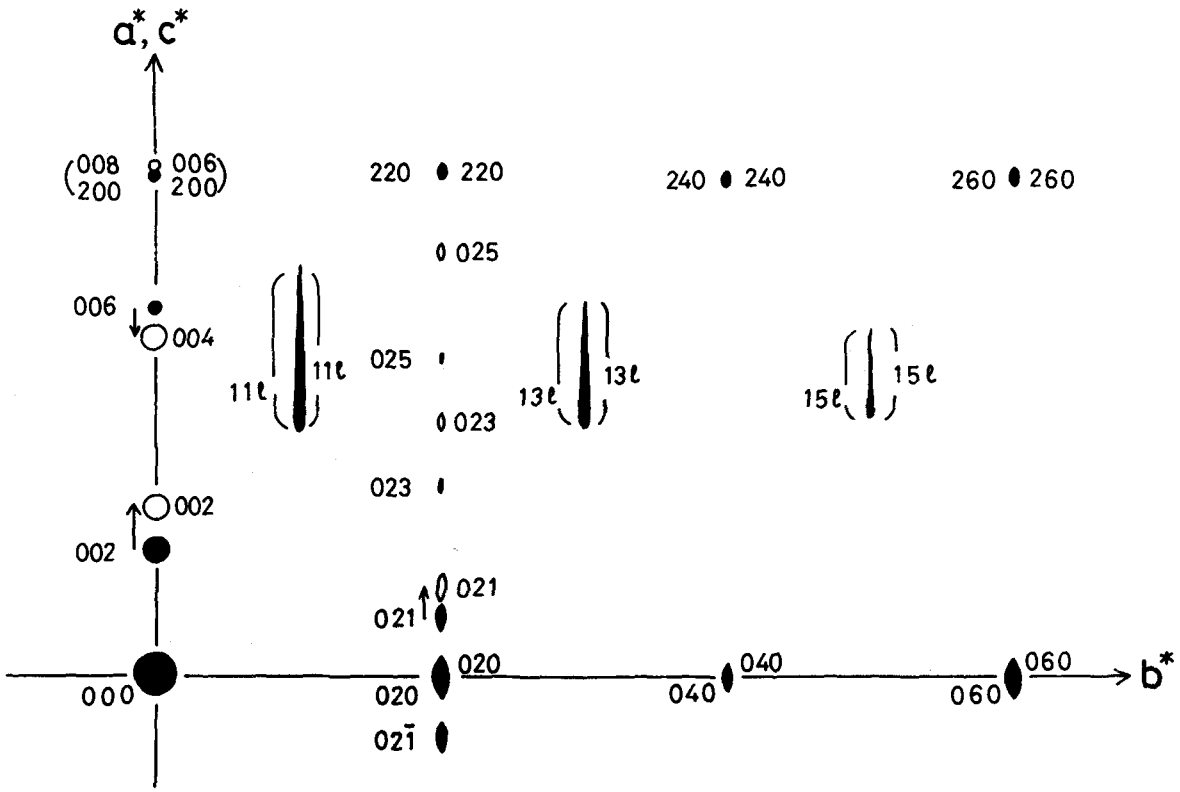


Fig. 8. Indices for observed SAED patterns from the halloysite tubes. Left side indices: halloysite (10 Å); right side indices: halloysite (7 Å).

– $\sigma_3$ which is the structure designated as I,3 by Zvyagin (1962). They deduced the structure on the basis of the calculated $|F|^2$-values of 02*l* and 11*l* reflections from the parameters of the unit cell obtained from the oblique texture electron diffraction patterns of halloysite (7 Å); $a$ = 5.14 Å, $b$ = 8.90 Å, $c$ = 14.7 Å, $\beta$ = 96°. The calculated $|F|^2$-values are in good agreement with their observed intensity distribution of 02*l* reflections where 0,2,2*l* + 1 reflections are enhanced compared to 0,2,2*l*($l \neq 0$). The observed intensity distribution of 02*l* for halloysite (7 Å) by the present study also shows a good agreement with this relationship, whereas the observed $\beta$-angle is about 102° which is similar to 104° and is obviously different from the value taken on the basis of the calculation by Chukhrov and Zvyagin (1966), by whom the structure of halloysite (7 Å) was reported to produce the ideal $\beta$-angle 96°. With regard to this contradiction, there seems to be present a possibility of another structure for halloysite (7 Å). It is, at least, obvious that the observed $\beta$-angle 102° is satisfied with the displacement of 2*a*/3 during one alternation of two-layer periodicity. As it is difficult to identify the halloysite structure only by the value of $\beta$-angle, the calculation of relative values $|F|^2$ for all the possible models, and the comparison to the models by Honjo and Mihama (1954) and Chukhrov and Zvyagin (1966), and to the other structures of kaolin minerals are by all means needed. They are now in progress and will be reported in the near future.

*Morphological changes due to dehydration of interlayer water*

Some morphological changes due to dehydration of interlayer water were clearly observed. Tubular halloysite of the present specimen is characterzied by particles with a considerable variation in diameters ranging from long narrow tubes to short ones (Figures 9a, b). Figure 9a was observed in wet air atmosphere [E.C. (air)] and Figure 9b in vacuum [E.C. (vac)]. By SAED analyses they were confirmed as the fully hydrated and the fully dehydrated forms of halloysite, respectively. The halloysite (10 Å) particles were observed as smooth and uniform contrast tubes, and no stripes could be recognized in the images except for a light center region, but in vacuum many dark and light stripes with widths of about 50 to 100 Å were observed along the tube axes.

The diameter of the halloysite tubes varies from 300 to 1200 Å with the maximum frequency around 500 Å (Figure 10[3]). The diameter seems to increase with the dehydration of the interlayer water. The diameter in a wet air atmosphere compared with that in vacuum is shown in Figures 10 and 11. In Figure 10 it is shown that the diameter difference varies from 0 to 30%. If the diameter were not changed, the points would plot on

https://doi.org/10.1346/CCMN.1978.0260103 Published online by Cambridge University Press

Table 3. Unit-cell data for halloysite (10 Å), halloysite (7 Å), and kaolin minerals.

| | $a_0$ (Å) | $b_0$ (Å) | $c_0$ (Å) | α | β | γ |
|---|---|---|---|---|---|---|
| Halloysite(10A) (Present specimen) | 5.14 | 8.90 | 20.7 | 90° | 99.7° | 90° |
| Halloysite(7A) (Present specimen) | 5.14 | 8.90 | 14.9 | 90° | 101.9° | 90° |
| " (Honjo, et al, 1954b) | 5.14 | 8.93 | 14.7 | 90° | 104° | 90° |
| " (Honjo, et al, 1954a) | 5.14 | 8.90 | 14.7 | 91.8° | 97° | 90° |
| " (Chukhrov, et al, 1966) | 5.14 | 8.90 | 14.7 | 90° | 96° | 90° |
| Kaolinite (Zvyagin, 1960) | 5.13 | 8.89 | 7.25 | 91°40' | 104°40' | 90° |
| Dickite (Newnham, et al, 1956) | 5.149 | 8.949 | 14.419 | 90° | 96°48' | 90° |
| " (Bailey, 1963) | 5.150 | 8.940 | 14.736 | 90° | 103°35' | 90° |
| Nacrite (Zvyagin, 1967) | 8.89 | 5.14 | 43.1 | 90° | 91°30' | 90° |

the line of $y = x$ in Figure 11. They plot instead on the line of $y = 1.12x$, and the increase in ratio of the diameter in vacuum against the diameter in wet air atmosphere was estimated around 10% (this data came from the black circles in Figure 10 [1]). These two phenomena, i.e., occurrence of stripes and expansion of the diameter in vacuum, are the main morphological changes discovered by "dynamic observation" of the electron microscope with E.C. In the following, the experimental results will be shown to explain the reason why these morphological changes occurred.

Figure 12 shows the results of "dynamic observation" obtained from another tubular mineral, namely clino-chrysotile, which has no interlayer water. The left figure was obtained in E.C. (air) and the right one in E.C. (vac). For the observation in vacuum the stripes and/or expansion of diameter could not be recognized, i.e., clino-chrysotile which has no interlayer water does not exhibit any morphological changes during "dynamic observation." The appearance of stripes and the expansion in diameter of halloysite in vacuum, therefore, must be caused by dehydration of the interlayer water.

It was confirmed also that the appearance of stripes is not related to irradiation by the electron beam. Halloysite (7 Å) particles previously dehydrated in a high vacuum were dispersed in water and dropped on the usual copper-grid, then observed by an electron microscope with the current density gradually increasing. Halloysite (7 Å) crystals having stripes did not show any changes through the observation, and when the electron dosage was increased considerably, the marginal parts of the crystals became unclear and showed smooth contrast like an amorphous material.

The electron microscopic image of halloysite (7 Å) crystal was taken also by means of a "through focus series" to determine whether the images of stripes were really represented by the amplitude contrast or were derived from the phase contrast (Figure 13). If the stripes in the images of halloysite (7 Å) were derived from the phase contrast, the contrasts of the stripes would be changed by means of the "through focus series." The stripes, however, did not show any changes in this series except for true focus image (Figure 13; $\Delta f \doteqdot 0$). Therefore, it is revealed that the stripes represent a real texture in or on the crystal.

The replica method was applied to determine whether the stripes represent a surface texture of halloysite crystals. As the result, the halloysite (7 Å) particles show smooth surfaces and almost rounded tubes which contrast with the polyhedral morphology of halloysite (7 Å) tubes observed by Chukhrov and Zvyagin (1966) and Dixon and Mckee (1974). No stripes or streaks could be recognized on the surface, so it is concluded that the stripes observed by transmission electron microscopic images exist as a real feature of the inner part of the halloysite (7 Å) crystal.

If some crevices exist in the inner part of the halloysite (7 Å) crystal, the contrast of the stripes observed in the electron microscopic image should be changed if a heavy metal layer is infiltrated into these crevices.

https://doi.org/10.1346/CCMN.1978.0260103 Published online by Cambridge University Press

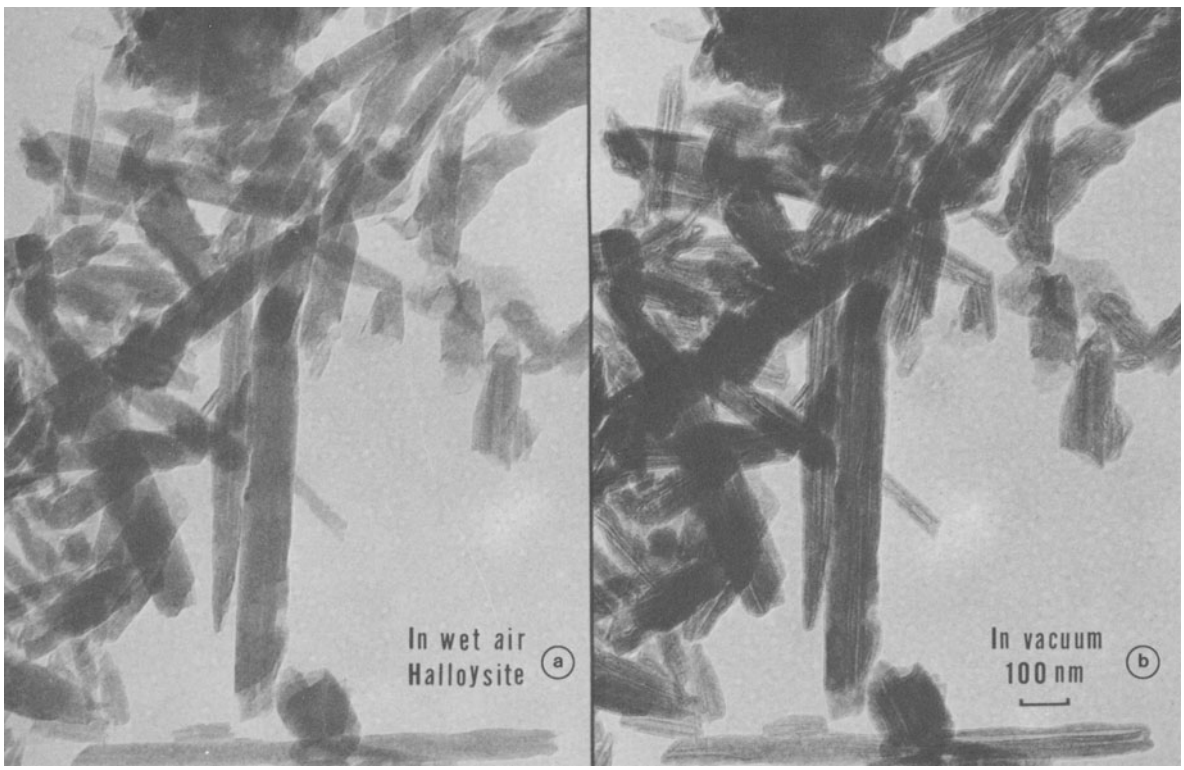


Fig. 9. Morphological changes of halloysite as observed by "dynamic observation." (a) halloysite (10 Å) observed in wet air atmosphere [E.C. (air)]; (b) halloysite (7 Å) observed in vacuum [E.C. (vac)].

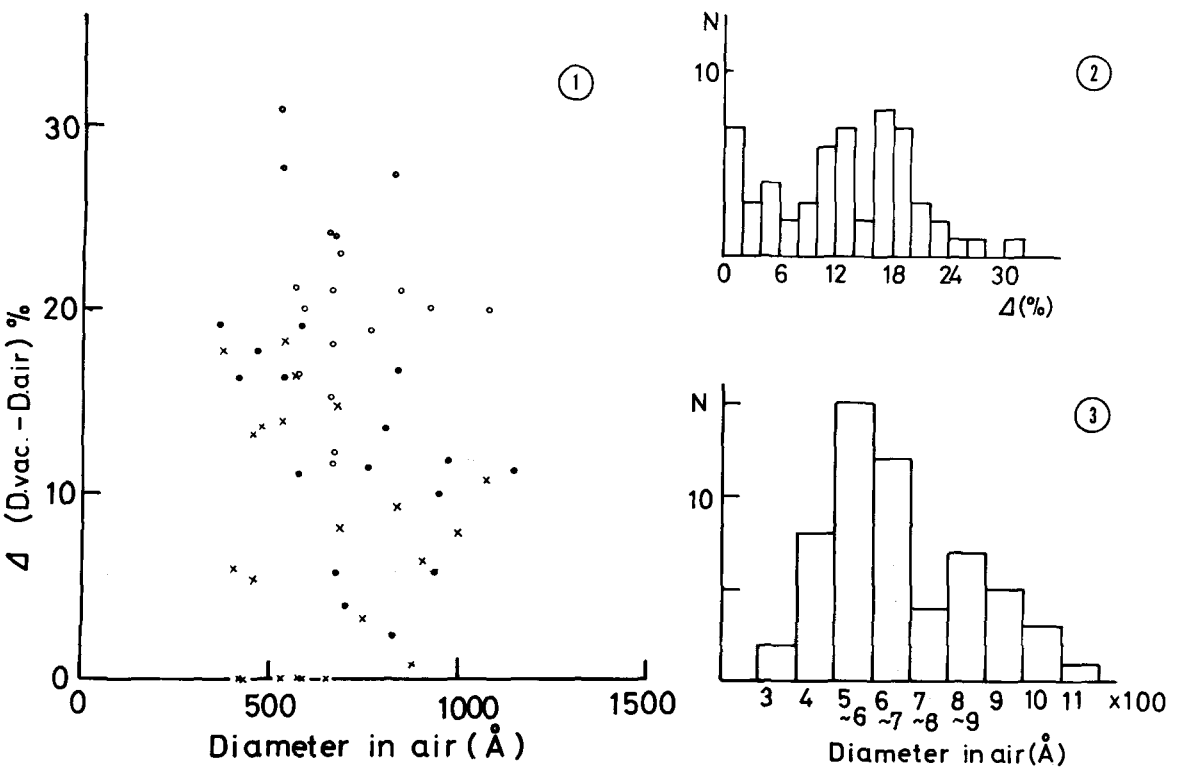


Fig. 10. Distribution of the halloysite tube diameters. Δ%, difference of diameter in vacuum against the diameter in wet air; N, number of observed particles.

https://doi.org/10.1346/CCMN.1978.0260103 Published online by Cambridge University Press

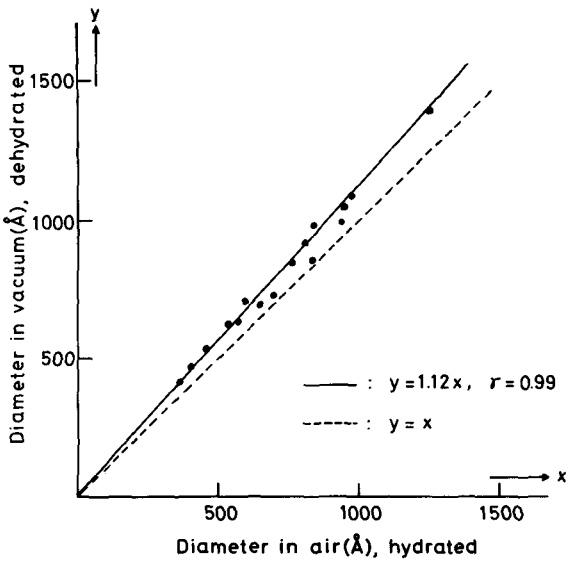


Fig. 11. Increasing ratio of the diameter of halloysite tubes in vacuum against the diameter in wet air.

The negative staining method usually used in the field of biology was applied for this purpose. The fully dehydrated form of halloysite was immersed in a saturated solution of uranyl acetate for a few days. After that, the halloysite (7 Å) particles were washed by pure water and observed by electron microscopy. As shown in Figure 14, the borders of the light center regions and of large crevices show especially dark contrast. Therefore, it is considered that the uranyl acetate layer has infiltrated into these crevices. These crystals show a smooth texture in contrast to be pretreated halloysite (7 Å) and seem to be similar to the images of halloysite (10 Å) rather than those of halloysite (7 Å). This result strongly suggests that some crevices exist in the inner part of the halloysite (7 Å) crystal because the contrast was changed by the treatment.

Other halloysite features observed in E.C. (air) and in E.C. (vac) are shown also in Figures 15a, b. In these figures, the end-views (cross-sectional views) of halloysite (10 Å) and halloysite (7 Å) can be seen in both the hydrated and dehydrated state. Enlarged end-views of halloysite (7 Å) are shown in Figure 15b. It can be seen that the tube is segregated into units of considerable thickness by the dehydration, and that crevices occur between these units. This unit is considered to correspond to the "packets" mentioned by Dixon and Mckee (1974).

Next, the crystallite thickness along the $c^*$-axis, L(002), was determined by a simple X-ray diffraction method to determine whether or not the segregation by dehydration makes the crystallite thickness smaller. Crystallite thickness is given by the Scherrer equation:

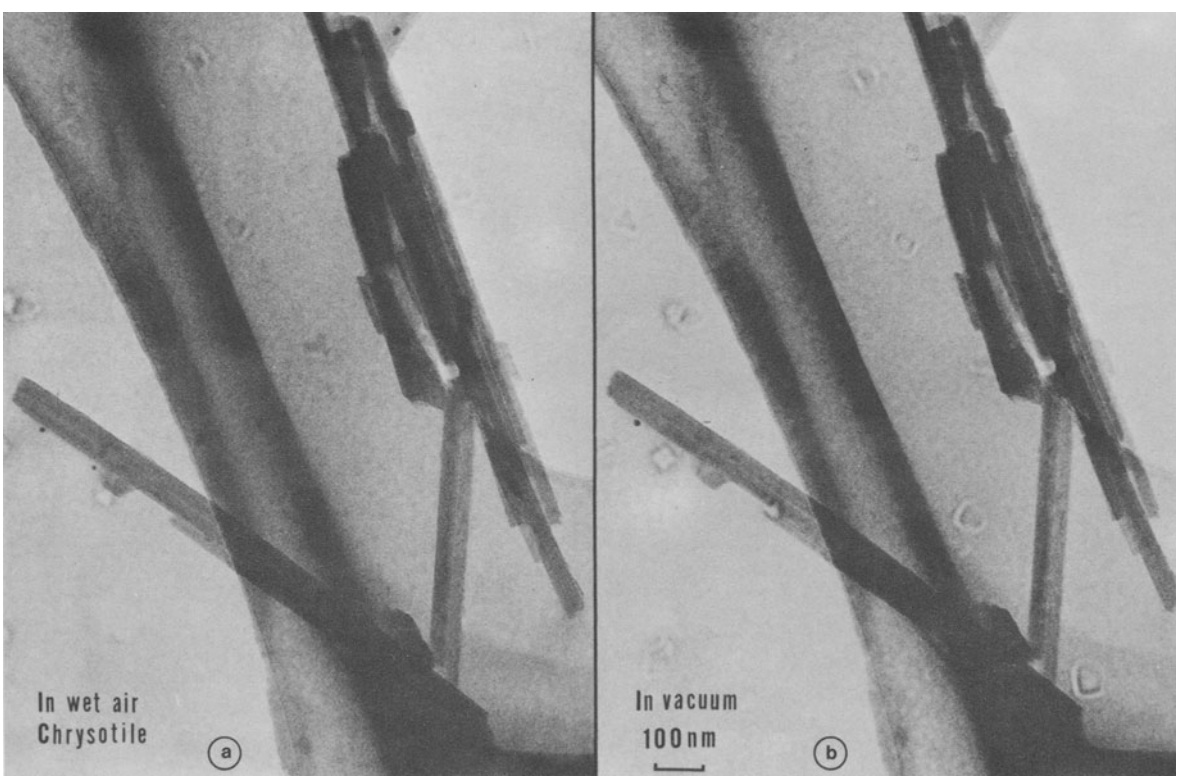


Fig. 12. The "dynamic observation" of clino-chrysotile, showing tubular particles. (a) observed in wet air atmosphere; (b) observed in vacuum.

https://doi.org/10.1346/CCMN.1978.0260103 Published online by Cambridge University Press

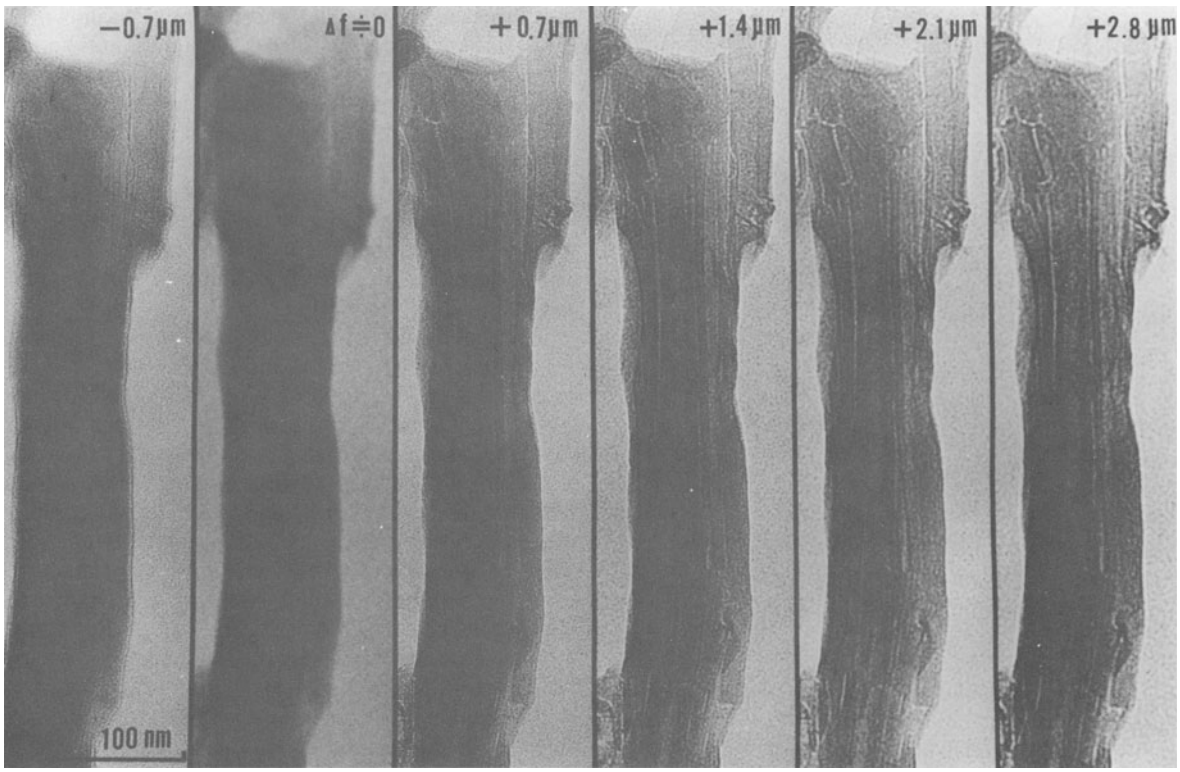


Fig. 13. Halloysite (7Å) particles observed by the "through focus series" with conventional electron microscope. −, overfocus; +, underfocus.

$$L = \frac{K\lambda}{\beta\cos\theta}$$

where L is crystallite thickness, λ is wave length of Cu $K_\alpha$, $\beta$ is half-width of X-ray diffraction peak, $\theta$ is diffraction angle, and K is a constant (in this analysis K = 1 was used for the sake of convenience). $\beta$ was modified by subtracting the instrumental broadening as determined by a thick crystal of muscovite. The results are shown in Table 4. As the $\beta$-values given in Table 4 include the effects of both crystallite thickness and lattice strain, the L(002) values also include both factors. But the latter is considered to be so small compared with the former (Iizuka and Kobayashi, 1975) that we call L(002) the crystallite thickness or "domain" for convenience in the following. The crystallite thicknesses of halloysite (10 Å) and halloysite (7 Å) are about 133 Å and 116 Å, respectively. The crystallite thickness of halloysite (7 Å) apparently seems to be just smaller than that of halloysite (10 Å). It would be caused mainly by the change of layer thickness from 20.7 to 14.9 Å, but the number of layer per crystallite thickness (N) is scarcely changed at all. It is concluded, therefore, that the segregation caused by dehydration does not affect the crystallite thickness, i.e., "domain" size along the *c*-axis direction. This means the segregation occurs in the same thickness as that of crystallite or scarcely larger than that.

On the basis of these experimental results, the idealized model of morphological changes by dehydration is shown in Figure 16. Halloysite layers are considered to be rolled spirally into tubes according to Figure 15 and to Dixon and Mckee (1974). In Figure 16, the left-hand side shows the hydrated form and right-hand side the dehydrated one. The upper pictures present the cross-sectional view and the lower the transmission electron micrograph image of the tubes. Each layer means a "unit" equivalent to the crystallite thickness ("domain") or just larger than the "domain," and the width of stripes observed in the images is just similar to the crystallite thickness. The "unit" consists of a small number of unit-cells of 20.7 Å or 14.9 Å thickness. The range of the number would be from 2 to 10 judging from the width of stripes (Figures 9, 15), X-ray diffraction analysis (Table 4), and the packet thickness reported by Dixon and Mckee (1974).‡ When halloysite is fully hydrated, the "domains" are tightly connected with each other, but become separated as a result of dehydration, and then can be seen as stripes along the tube axis in the transmitted image. This separation is caused by the shrinkage of the unit-cell from 20.7 to 14.9 Å, and each crystallite thickness also shrinks about

‡Dixon and Mckee (1974) calculated the number of unit-cells by dividing the packet thickness by a 7.2 Å layer, but it would be better if the packet thickness is divided by 14.4 Å layer because of the two-layer periodicity.

https://doi.org/10.1346/CCMN.1978.0260103 Published online by Cambridge University Press

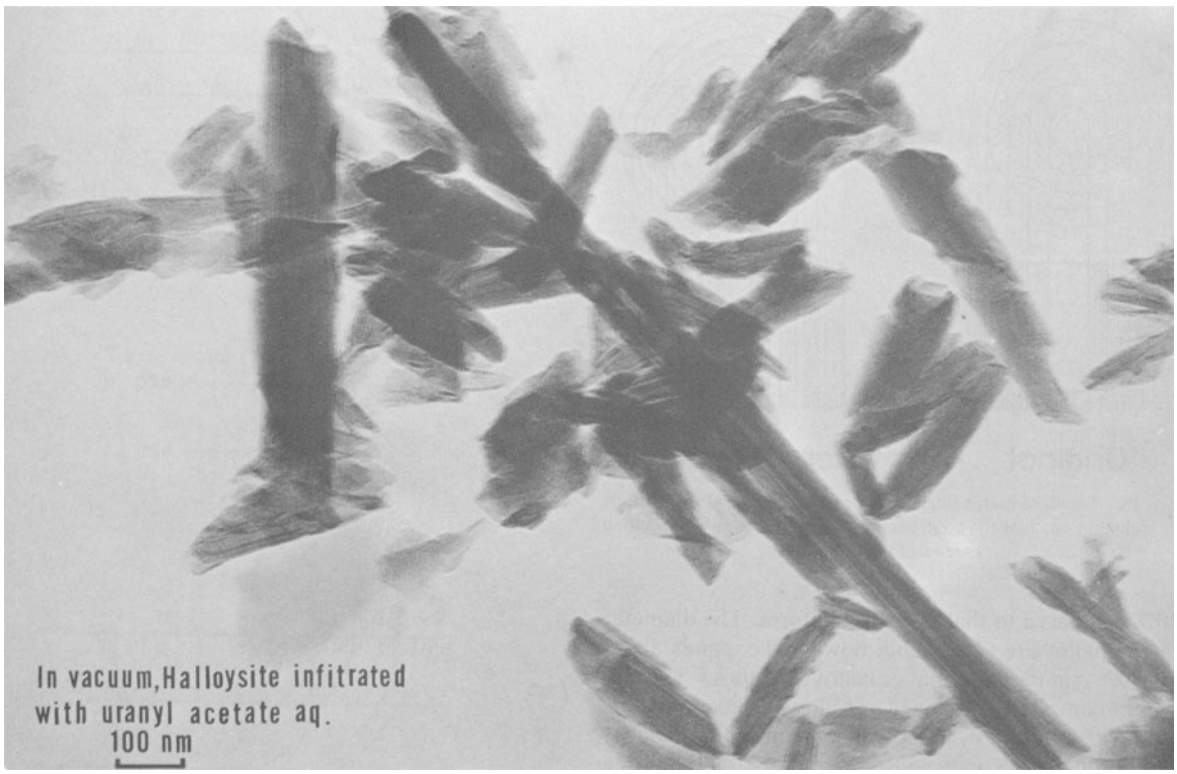


Fig. 14. Halloysite (7 Å) infiltrated with uranyl acetate aqua.

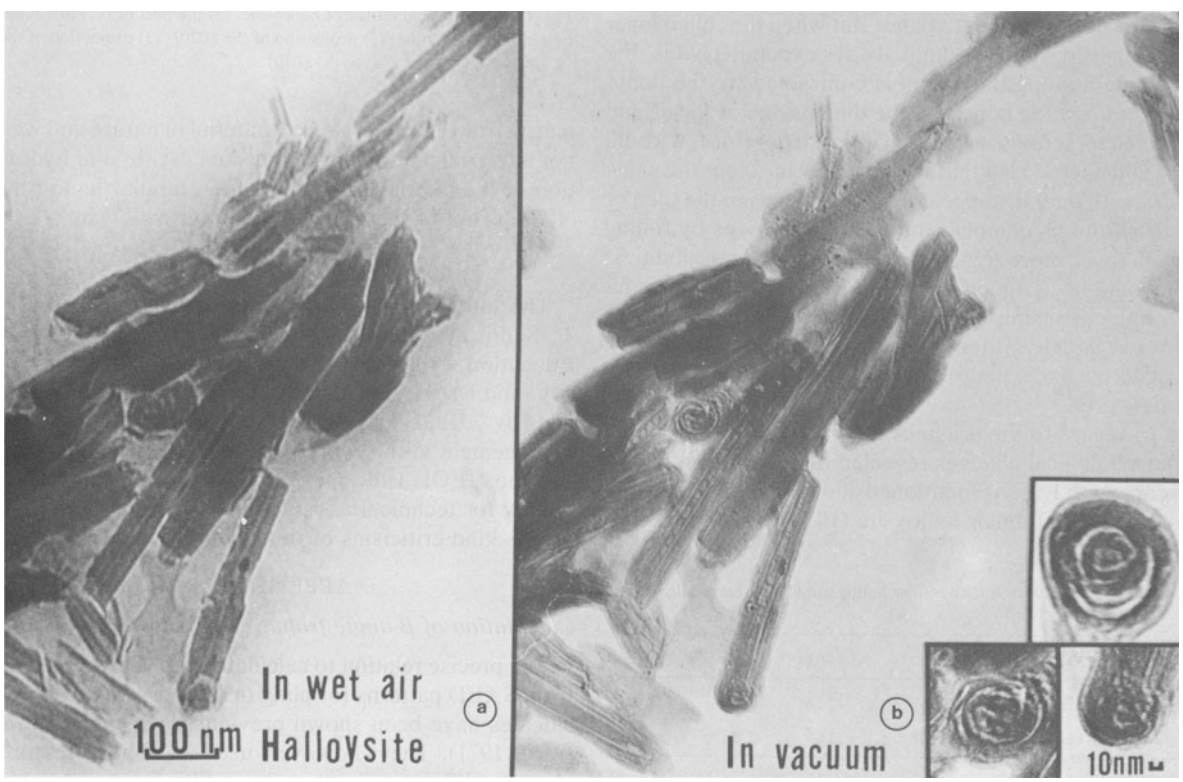


Fig. 15. Halloysite (10 Å) and halloysite (7 Å) particles observed by "dynamic observation." The edge views (cross-sectioned views) of halloysite (10 Å) and halloysite (7 Å) can be observed in both (a) and (b), and that of the latter enlarged in (b) (insert).

https://doi.org/10.1346/CCMN.1978.0260103 Published online by Cambridge University Press

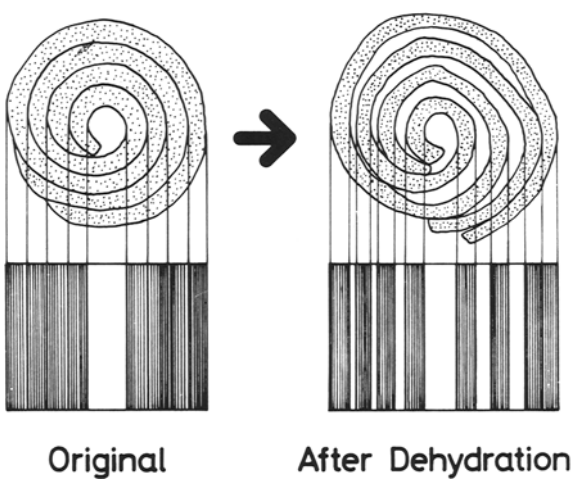


Fig. 16. Idealized morphological change of halloysite (10 Å) particle by dehydration. Upper—cross-sectional views; Lower—transmitted views of the tubes.

30% compared to that of hydrated form. The diameter of the halloysite (7 Å) tube, however, expands about 10–20% compared to that of halloysite (10 Å). This apparent contrast is explained as follows: Accompanying the layer separation, the rolled configuration of halloysite gradually becomes loose since the attractive force between the layers are weakened by the occurrence of crevices. As a result the diameter of halloysite (10 Å) tube is considered to expand. But when the rolled layer becomes loose, it need not always expand. That is, the thickness along the *c*-axis is contracted by the dehydration. On the contrary, the dimensions of the *a*- and *b*-axes directions are not changed. Therefore, it could be considered also that the diameter has kept the same size with only the appearance of crevices in the tube or has shrunk in compensation for the crevices by rolling each layer more tightly. In these various possibilities, it would be assumed that there is an inherent strain favoring expansion when the rolled configuration of halloysite is dehydrated, which is something like a book rolled by one's hand that expands upon relaxation of one's grip.

In regard to the origin of tubular halloysite from the morphological changes revealed by an electron microscope with E.C. as mentioned above, it is strongly considered that tubular halloysite (10 Å) was formed primarily from a certain source material in nature and was not altered from tubular halloysite (7 Å) by the hydration of the interlayer water, that is, tubular halloysite (10 Å) is not of secondary origin after halloysite (7 Å).

Table 4. Crystallite thickness for halloysite (10 Å) and halloysite (7 Å).

| | β(002) | L(002) | N |
|---|---|---|---|
| Halloysite(10Å) | 0.666° | 133Å | 7 |
| Halloysite(7Å) | 0.768° | 116Å | 8 |

N : Number of unit-cell layers per L(002). Each number was calculated with $L(002)/c_0$.

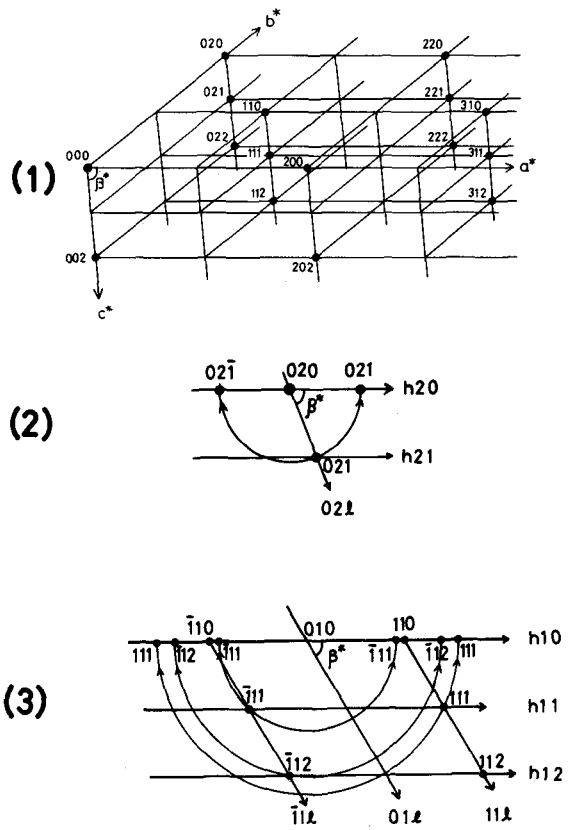


Fig. 17. Reciprocal lattice of halloysite. (1) the part of reciprocal lattice of halloysite tube; (2) projection of the {020}; (3) projection of the {010}.

## ACKNOWLEDGMENTS

The authors would like to express their thanks to Dr. T. Sudo, emeritus professor of Tokyo University of Education, Professor K. Nagasawa of Nagoya University, and Dr. H. Yotsumoto, Appl. Dep. Electron Optics Div., JEOL Ltd. for valuable suggestions and encouragement in this work. Thanks are also due to Mr. A. Ono, JEOL Ltd. and Mr. T. Kimura, Nihon University for technical assistance, and Dr. W. D. Keller for his kind criticisms of this manuscript.

## APPENDIX

### *Calculation of β-angle from SAED pattern*

The precise relation to calculate the lattice constants from SAED patterns for platy or fiber crystals of sheet silicates have been shown previously (Zvyagin, 1967; Gard, 1971). They, however, used an oblique texture electron diffraction pattern by a tilting apparatus for taking the (*h*0*l*) and/or (*hkl*) reflections because the cal-

https://doi.org/10.1346/CCMN.1978.0260103 Published online by Cambridge University Press

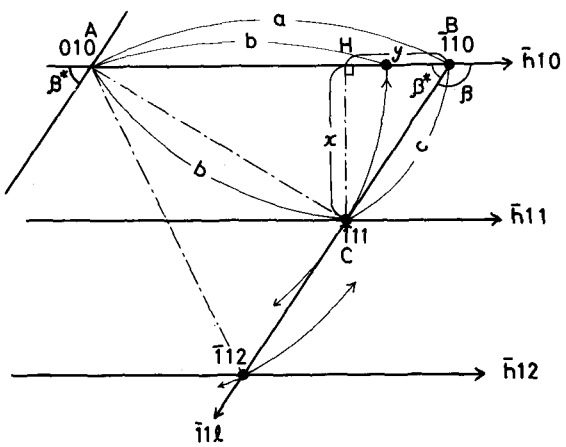


Fig. 18. Reciprocal lattice of halloysite. The notations are used for the calculation of lattice constants.

culation needed these d-spacings. On the SAED pattern of halloysite, $(h0l)$ or $(hkl)$ diffractions appear without a tilting apparatus but the high order $l$-values usually show streaky spots and the precise positions are unclear. Therefore, it is impossible to calculate the lattice constant from these relations. We propose a new calculation method in the following.

Figure 17(1) shows a reciprocal lattice of halloysite. The tube axis of halloysite is along the $b^*$-direction because the $b$-axis and $b^*$-direction coincide. The cross-sectional view shown in Figure 16 is, therefore, perpendicular to $b^*$-axis. The $a^*$- and $c$-axes are present around $b^*$-axis because of the rotational symmetry of the halloysite tube. Figure 17(2) shows the projection of the reciprocal lattice down $b^*$, and $c$-axis parallel to the electron beam. The Ewald sphere coincides with $[h20]$, and $[02l]$ rotates around $[0k0]$ because the halloysite tube has rotational symmetry. Therefore, when $[02l]$ cuts the Ewald sphere, i.e., $[h20]$, the reflections occur that form the diffraction pattern. It is obvious that the distance between the 020 and 021 spots is equal to $C_0\sin\beta$. Figure 17(3) shows the projections of the reciprocal lattice down $b^*$ with the electron beam parallel to the $c$-axis. Each spot in the $11l$ or $\bar{1}1l$ rows revolves around [010], so that the spots appear near the 110 or $\bar{1}10$ spots. It is clearly observed that the order of $11l$ spots is not in order of $l$-values. For example, in this case the order from 010 to the right side is $\bar{1}11$, 110, $\bar{1}12$, 111, and so on. Usually these diffraction spots do not appear as spots but as streaks, and the nearest end of the streak may correspond to $\pm\bar{1}11$.

The position of the $11l$ streak changes with layer thickness and with $\beta$-angle. The layer thickness depends upon dehydration of the interlayer water. As the $\beta$-angle changes towards 90°, the $\pm\bar{1}11$ spot moves to the 110 spot and passes over it at a certain angle, so that the $\beta$-angle may be calculated from the $\pm\bar{1}11$ position as shown in Figure 18.

Figure 18 shows the reciprocal lattice with the Ewald sphere corresponding with the $[\bar{h}10]$ direction. In Figure 18, $a$, $b$, and $c$ are the distances between 010 and $\bar{1}10$, 010 and $\bar{1}11$, and $\bar{1}10$ and $\bar{1}11$, respectively. The positions of 010, $\bar{1}10$, and $\bar{1}11$ are named $A$, $B$, and $C$, respectively. The foot of a perpendicular from $\bar{1}11$ to $[\bar{h}10]$ is named $H$. $x$ and $y$ stand for the distance of $CH$ and $BH$, respectively. The $\beta$-angle can be calculated from the following equations:

$$x^2 + (a - y)^2 = b^2 \quad (1)$$

$$x^2 + y^2 = c^2 \quad (2)$$

$$\tan\beta^* = \frac{x}{y}. \quad (3)$$

From (1) and (2),

$$y = \frac{a^2 - b^2 + c^2}{2a}$$

and

$$x = \sqrt{c^2 - y^2}.$$

From (3),

$$\beta^* = \tan^{-1}\frac{x}{y}.$$

$\beta^*$, therefore, can be calculated with the values of $x$ and $y$, and $\beta$ is expressed as $\beta = \pi - \beta^*$. $a$ and $c$ correspond with $K/a_0\sin\beta = K/d_{100}$ and $k_0\sin\beta = K/d_{100}$, respectively. K is constant.

In actual calculation, $a$ and $c$ are used as the distances between the 200 and $\bar{2}00$ spots, and the 002 and $00\bar{2}$ spots on the diffraction pattern, respectively. $b$ is the nearest distance between the $11l$ and $\bar{1}1l$ streaks on the diffraction pattern.

As an example, d-spacings of some $02l$ and $\pm\bar{1}1l$ reflections were calculated using the observed unit-cell parameters obtained by the above method. They are as follows: Halloysite (10 Å); 020 = 4.45 Å, $\bar{1}11$ = 4.44 Å, 110 = 4.40 Å, 021 = 4.35 Å, $\bar{1}12$ = 4.27 Å, 111 = 4.18 Å; Halloysite (7 Å); 020 = 4.45 Å, $\bar{1}11$ = 4.42 Å, 110 = 4.38 Å, 021 = 4.26 Å, $\bar{1}12$ = 4.12 Å, 111 = 4.02 Å. The order from 010 to the right side in Figure 17(3) well coincides with these calculated results.

## REFERENCES

A.I.P.E.A. (1975) Meeting of the nomenclature committee of A.I.P.E.A. (in Mexico City): *Clays & Clay Minerals* **23**, 413–414.

Askenasy, P.E., Dixon, J. B. and Mckee, T. R. (1973) Spheroidal halloysite in a Guatemalan soil: *Soil Sci. Soc. Am. Proc.* **37**, 799–803.

Bailey, S. W. (1963) Polymorphism of the kaolin minerals: *Am. Mineral.* **48**, 1196–1206.

Bates, T. F. (1971) The kaolin minerals. In *The Electron-Optical Investigation of Clays* (Edited by Gard, J. A.), pp. 109–157: Mineral. Soc., London.

Bates, T. F., Hildebrand, F. A. and Swineford, A. (1954) Morhpology and structure of endellite and halloysite: *Am. Mineral.* **35**, 463–484.

Brindley, G. W. (1961) Kaolin, serpentine and kindred minerals. In

https://doi.org/10.1346/CCMN.1978.0260103 Published online by Cambridge University Press

*The X-ray Identification and Crystal Structures of Clay Minerals* (Edited by Brown, G.), pp. 51–131: Mineral. Soc., London.

Brindley, G. W. and Nakahira, M. (1958) Further consideration of the crystal structure of kaolinite: *Mineral. Mag.* **31,** 781–786.

Brindley, G. W. and Robinson, K. (1946) The structure of kaolinite: *Mineral. Mag.* **27,** 242–253.

Chukhrov, F. V. and Zvyagin, B. B. (1966) Halloysite, a crystallochemically and mineralogically distinct species: *Proc. Int. Clay Conf.*, Jerusalem **1,** 11–25.

Dixon, J. B. and Mckee, T. R. (1974) Internal and external morphology of tubular and spheroidal halloysite particles: *Clays & Clay Minerals* **22,** 127–137.

Dorset, D. J. and Parsons, D. F. (1975) Electron diffraction from single, fully-hydrated, ox-liver catalase microcrystals: *Acta Crystallogr.* **A31,** 210–215.

Drits, V. A. and Kashaev, A. A. (1960) An X-ray study of a single crystal of kaolinite: *Kristallografiya* **5,** 224–227 (Eng. transl. pp. 207–210).

Fukami, A. and Katoh, M. (1972) Construction and application of environmental cell: *Proc. 30th EMSA Meeting*, 614–615.

Fukami, A. and Murakami, S. (1974) Observation of hydrated materials using environmental cell and its application: *Electron Microscopy* **9,** 4–19 (In Japanese).

Fukami, A., Fukushima, K. and Murakami, S. (1974) Observation technique of hydrated biological material using environmental cell: *Proc. 8th Int. Congr. Electron Microscopy*, Canberra, **2,** 45–46.

Gard, J. A. (1971) Interpretation of electron micrographs and electron-diffraction patterns. In *The Electron-Optical Investigation of Clays* (Edited by Gard, J. A.), pp. 27–78: Mineral. Soc., London.

Honjo, G. and Mihama, K. (1954) A study of clay minerals by electron-diffraction diagrams due to individual crystallites: *Acta Crystallogr.* **7,** 511–513.

Honjo, G., Kitamura, N. and Mihama, K. (1954) A study of clay minerals by means of single-crystal electron diffraction diagram—the structure of tubular kaolin: *Clay Miner. Bull.* **2,** 133–141.

Iizuka, M. and Kobayashi, K. (1975) On the crystallite thickness and interlayer spacing in some kaolin minerals. In *Contributions to Clay Mineralogy* (Dedicated to Prof. T. Sudo, On the Occasion of His Retirement), pp. 23–25 (in Japanese with English abstract).

Nagasawa, K., Takeshi, H., Fujii, N. and Hachisuka, E. (1969) Occurrence, properties and uses of the clays and allied minerals in Japan—Kaolin minerals (Edited by Editorial Subcommittee for "The Clays of Japan" Organizing Committee 1969 International Clay Conference in Tokyo), pp. 17–70. Geological Survey of Japan, Tokyo.

Newnham, R. E. (1961) A refinement of the dickite structure and some remarks of polymorphism in kaolin minerals: *Mineral. Mag.* **32,** 683–704.

Newnham, R. E. and Brindley, G. W. (1966) The crystal structure of dickite: *Acta Crystallogr.* **9,** 759–764.

Parsons, D. F. (1974) Structure of wet species in electron microscopy: *Science* **186,** 407–414.

Souza Santos, P. de, Brindley, G. W. and Souza Santos, H. de (1965) Mineralogical studies of kaolinite—halloysite clays: Part III. A fibrous kaolin mineral from Piedade, São Paulo, Brazil: *Am. Mineral.* **50,** 619–628.

Sudo, T. and Ossaka, J. (1952) Hydrated halloysite from Japan: *Jpn. J. Geol. Geogr.* **22,** 215–229.

Zvyagin, B. B. (1960) Electron-diffraction determination of the structure of kaolinite: *Kristallografiya* **5,** 40–50 (Engl. transl. pp. 32–42).

Zvyagin, B. B. (1967) *Electron-diffraction Analysis of Clay Mineral Structure* (Revised Edition): Plenum Press, New York.

Резюме- Гидратная форма трубчатого галлуазита /галлуазит (10Å)/ исследовалась под обычном электронным микроскопом,снабженным микросетчатой камерой /М.К./,благодаря чему была выявлена "естественная" форма без дегидратации межслойной воды.Эта статья посвящена анализу методом электронной дифракции избранной зоны /ЭДИЗ/ галлуазита и его морфологических изменений в результате дегидратации.Рисунок ЭДИЗ показал,что галлуазит (10Å) имеет двухслойную периодичность в моноклинальной структуре с параметрами единичной ячейки $a$=5,14Å,$b$=8,90Å,$c$=20,7Å,β=99,7° в пространственной группе $Cc$ и почти такую же структуру,как обезвоженная форма галлуазита /галлуазит (7Å)/.Это означает,что дегидратация межслойной воды не изменяет и не воздействует значительно на структуру галлуазита (10Å).Впроцессе дегидратации межслойной воды вдоль осей трубок появились светлые полосы шириной около 50-100Å.Диаметры трубчатых частиц также увеличились примерно на 10%.В результате различных экспериментов,таких как серии фокусировок,наблюдение поверхностной структкры методом репродукции,наблюдение торцов трубчатых частиц и других, этот феномен объясняется следующим образом.Кристаллы галлуазита имеют "домены",направленные вдоль осей $c$,толщина "доменов" варьирует в педелах 50-100Å.Они тесно связаны друг с другом,когда галлуазит насыщен водой,но разделяются в результате дегидратации межслойной воды,и тогда появляются полосы вдоль осей трубок.Принимая во внимание эти соображения,предлагается модель дегидратации.Более того,в приложении предлагается метод вычисления угла β.

https://doi.org/10.1346/CCMN.1978.0260103 Published online by Cambridge University Press